Flow-field development during finger splitting at an exothermic chemical reaction front

L. Šebestíková,[1,*,†] J. D'Hernoncourt,[2,*,‡] M. J. B. Hauser,[1,§] S. C. Müller,[1] and A. De Wit[2,‖]
[1]*Institut für Experimentelle Physik, Abteilung Biophysik, Otto-von-Guericke-Universität Magdeburg, Universitätsplatz 2, 39106 Magdeburg Germany*
[2]*Nonlinear Physical Chemistry Unit and Center for Nonlinear Phenomena and Complex Systems, CP 231, Université Libre de Bruxelles, 1050 Brussels, Belgium*
(Received 12 September 2006; published 22 February 2007)

Fingertip splitting may be observed at chemical reaction fronts subject to buoyancy-induced Rayleigh-Taylor fingering, as investigated in ascending fronts of the iodate-arsenous acid reaction in vertical Hele-Shaw cells. We study the properties of the flow-field evolution during a tip-splitting event both experimentally and theoretically. Experimental particle-image velocimetry techniques show that the flow field associated to a finger displays a quadrupole of vortices. The evolution of the flow field and the reorganization of the vortices after a tip-splitting event are followed experimentally in detail. Numerical integration of a model reaction-diffusion-convection system for an exothermic reaction taking into account possible heat losses through the walls of the reactor shows that the nonlinear properties of the flow field are different whether the walls are insulating or conducting. In insulating systems, the flow field inside one finger features only one pair of vortices. A quadrupole of flow vortices arranged around a saddle-node structure similar to the one observed experimentally is obtained in the presence of heat losses suggesting that heat effects, even if of very small amplitude, are important in understanding the nonlinear properties of fingering of exothermic chemical fronts.

DOI: 10.1103/PhysRevE.75.026309 PACS number(s): 47.70.Fw, 47.20.Bp, 47.80.Jk, 82.40.−g

I. INTRODUCTION

The coupling between autocatalytic chemical reactions and molecular diffusion can lead to a chemical front of products invading the reactants. If the density changes across such a moving autocatalytic reaction-diffusion (RD) front lead to a stratification of a heavier solution placed on top of a lighter one in the gravity field, it can lead to Rayleigh-Taylor instabilities [1–3]. In the present paper we focus on the iodate-arsenous acid (IAA) reaction known to generate chemical RD fronts and to display a density decrease due to the change in the chemical composition during the reaction. In this reaction the products are thus less dense than the reactants leading to a Rayleigh-Taylor instability at the chemical front that travels upwards. This fingering instability of the IAA reaction has been investigated thoroughly in experiments and theory. First, in capillary tubes [4,5] where the fronts traveling upward are no longer flat beyond a critical capillary diameter. The related modifications of the front velocity due to convection were analyzed and compared to the velocity of purely reaction-diffusion fronts. The limited diameters of capillary tubes provided only sufficient space for the formation of one or two convection rolls around the front. To let more fingers develop, Hele-Shaw cells [6–9] were used enabling an easy visualization of the finger development in spatially extended fronts. In this geometry, different studies have focused first on the early stages of the instability providing dispersion curves (that determine the growth rate of the perturbations as a function of their wave numbers) revealing information about both the time of apparition and the wavelength [7,9,10] of the fingering pattern. After their generation, the fingers grow and interact with each other driving the instability into the nonlinear regime. In this regime, both experimental [8] and theoretical [3] studies have shown that, after the initial formation of the pattern, the fingers tend to merge leading to larger fingers. The numerical integration of a model for isothermal fingering of IAA fronts has pointed out that this coarsening can lead to a single finger of constant length, which grows at a constant speed. However, if the finger grows large enough it tends to split at the tip generating two or more smaller fingers from a bigger one [3]. A recent numerical study [11] has shown that if the Hele-Shaw cell is not perfectly insulated, heat losses through the reactor walls enhance the tip-splitting phenomenon.

In this context, the purpose of the present paper is to examine in more detail both experimentally and theoretically the tip-splitting phenomena occurring during the nonlinear regime of the fingering. In particular, we wish to focus on the convective movements of the fluid associated with the finger splitting. Experimentally, the flow during fingering of IAA fronts has been studied in a Hele-Shaw cell by particle-image velocimetry (PIV), which allows one to visualize the hydrodynamic flow fields before, during, and after the splitting of a reaction front. Since the fluctuations in the mass transport across the reaction front that lead to finger splitting occur in minute areas at the finger tip, it may often be difficult to resolve these fluctuations by PIV analysis. Finger splitting causes a rearrangement of the macroscopic flow field at the splitting front and its vicinity. This rearrangement is found to take some time (60–80 s) until it is fully established. In our theoretical considerations, we study numerically the nonlinear finger dynamics of a RD front system in both the pres-

*These authors contributed equally to this work.
†Electronic address: lenka.sebestikova@physik.uni-magdeburg.de
‡Electronic address: jdhernon@ulb.ac.be
§Electronic address: marcus.hauser@physik.uni-magdeburg.de
‖Electronic address: adewit@ulb.ac.be

ence and absence of heat losses through the walls. As a model system we use a one-variable RD model known to describe the IAA reaction for the experimental conditions used here coupled to Darcy's equation to account for the flow velocity in the Hele-Shaw cell. We show that the thermal leaks through the walls of the cell lead to the presence of thermal pulses and to squeezed vorticity, which influences the convection rolls in the bulk leading to increased finger splitting.

This paper is organized as follows. In Sec. II we present the experimental results of the visualized flow fields before, during, and after finger splitting. In Sec. III the theoretical model is introduced and an analysis of the effect of the heat losses through the walls on the nonlinear fingering phenomena and on the characteristics of the flow field is performed. The experimental and numerical results are compared and discussed in Sec. V and conclusions are put forward in Sec. VI.

II. EXPERIMENTS

A. The iodate-arsenous acid reaction

The reaction studied is the autocatalytic oxidation of arsenous acid by iodate, the so-called IAA reaction, which supports propagating chemical fronts in spatially distributed media [12,13]. The oxidation of arsenous acid by iodate consists of two coupled steps, each of which consumes a product formed in the other reaction, i.e., I_2 and I^-, respectively.

$$IO_3^- + 5I^- + 6H^+ \rightarrow 3I_2 + 3H_2O, \tag{1}$$

$$H_3AsO_3 + I_2 + H_2O \rightarrow 2I^- + H_3AsO_4 + 2H^+. \tag{2}$$

Both the net stoichiometry of the overall reaction and the composition of the reacted solution depend on R, the ratio of the initial concentrations of reactants,

$$R = \frac{[H_3AsO_3]_0}{[IO_3^-]_0}. \tag{3}$$

Three cases of initial concentration ratios R may be considered, since they lead to substantially different chemical compositions of the reacted solutions [14]. In the first case arsenous acid is present in stoichiometric excess over IO_3^-, which occurs for $R>3.0$. Here, IO_3^- is completely consumed, I_2 is an intermediate, and I^- is a reaction product. Second, for $3>R>2.5$, the two reactants H_3AsO_3 and IO_3^- are completely consumed and I^- as well as I_2 are the final products. Finally, for $R<2.5$, iodate is present in stoichiometric excess over the arsenous acid, and H_3AsO_3 is completely consumed, while I^- is an intermediate, and I_2 is a reaction product.

B. Experimental procedure

All experiments were carried out at the ratio of initial concentrations $R=3.2$, where arsenous acid is present in stoichiometric excess over IO_3^- and I_2 occurs as an intermediate. The status of the reaction was made visible by the addition of starch as an indicator (0.06% w/v), which forms a colored complex with I_3^-, thus indicating the loci of high I_2 concentrations. The reaction can be followed as a propagating thin dark blue reaction front that separates the colorless solutions of reactants and products from each other. The room temperature was kept constant at (21 ± 1) °C and varied at most by ±0.2 K during one experiment. All solutions were equilibrated at room temperature for at least two hours prior to the start of the experiment. Reaction mixtures contained 0.016 mol l^{-1} $NaAsO_2$, 0.016 mol l^{-1} H_2SO_4, 0.005 mol l^{-1} $NaIO_3$, 0.06% w/v starch, and 0.01% w/v latex particles (average diameter 5 μm), and were prepared freshly from degassed stock solutions.

The experiments were performed in a vertically oriented Hele-Shaw cell, which consists of two glass plates (30×30 cm^2) separated by a 0.5 mm Teflon spacer. Two conductive stripes of indium-tin-oxide (ITO) coated on one of the glass plates were used to initiate planar reaction fronts electrochemically by a potential difference of −3.5 V. The dc electric field was applied until a pair of planar reaction fronts, one ascending, the other descending, were fully formed. Frontal illumination of the Hele-Shaw cell was achieved by a cold light source.

The progress of the experiments was recorded with a charge-coupled device camera connected to a computer where the incoming data were stored digitally at a frequency of 1 Hz using a commercial frame grabber. Particle image velocimetry (PIV) of buoyant latex particles was performed to visualize and evaluate the hydrodynamic flow fields. The flow vectors were reconstructed from pairs of digitized images, each $\Delta t=6$ s apart from each other. The displacement of the particles was calculated as the maximum of the cross-correlation function between the same interrogation window in two subsequent images. The size of the pixel interrogation windows was 40×40 $pixels^2$.

Even though the used Hele-Shaw cell was large, the total size of the observation area was restricted to a relatively small domain, which monitors only one of the fingers of the ascending reaction front at a time. Each finger studied was located at least 5 cm from the edge of the Hele-Shaw cell in order to avoid any influences from the boundaries. The limitation in the size of the detection domain results from the requirement that the tracer particles and the reaction front must be monitored simultaneously, thus allowing for the detection of both the front dynamics and the associated hydrodynamic flows. Since one pixel may not represent an area that is larger than that of a tracer particle, the maximum size of the observation area is restricted to 1.87×0.97 cm^2. To record the temporal development of both the reaction front and the concomitant hydrodynamic flow field the camera was repositioned when the ascending reaction front reached the top of the observation window, such that the top of the reaction front was in the bottom of the new observation window.

C. Experimental results

Once the reaction was initiated at the ITO cathode, two traveling reaction fronts formed. The downward propagating front is flat and its shape is stable while the ascending front

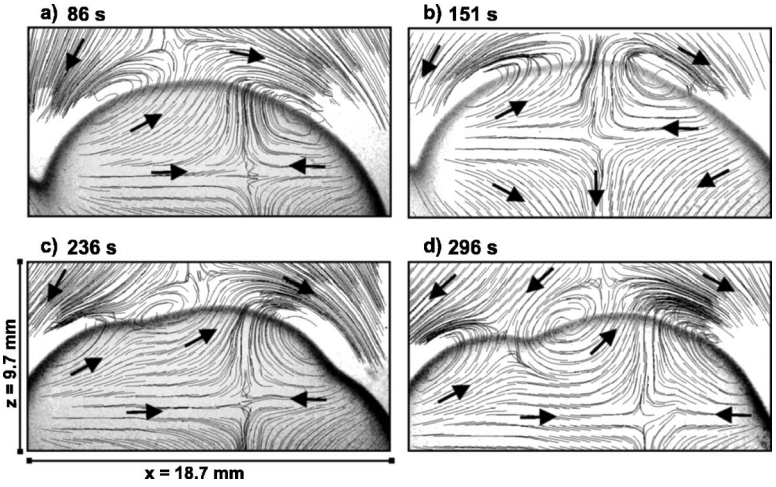

FIG. 1. Fingertip splitting and the adjacent flow field. (a) At 86 s a fully developed finger is accompanied by two convection rolls at the front. The flow streams at the very bottom suggest the existence of a second pair of vortices in a deeper position of the liquid layer. (b) At $t \sim 151$ s the finger starts to split while the macroscopic flow-field pattern is quite reminiscent of the situation prior to finger splitting. (c) At $t \sim 236$ s the splitting is clearly seen. The macroscopic flow field is being rearranged. (d) Finally, at $t=296$ s the new fingers and the rearranged macroscopic flow field is fully developed. The bold arrows indicate the general direction of the flow field.

is buoyantly unstable. After some time, the upward propagating front distorts and fingers are formed. The later stage of finger development, i.e., the nonlinear regime, is characterized by finger merging, coarsening, and splitting. Splitting occurs at the top of the fastest growing fingers. The evolution of fingers is associated with an induced hydrodynamic flow, which also develops in time. The temperature difference between the wave front and the ambient (reacted and unreacted) solutions were measured to be in the order of $\Delta T \leqslant 0.1$ K. The dynamics of the dominant fingers were followed in order to monitor the flow-field development and finger splitting.

A typical example of a flow field during the splitting of a dominating finger is shown in Fig. 1. The original images of the reaction front are overlayed by images of the corresponding flow fields, thus containing information about the shape and position of the reaction front as well as the associated hydrodynamic flow fields. The dark arcs in the images represent a section of the ascending reaction front, while thin curves are streamlines of the flow field. The general direction of flows is indicated by bold arrows.

Characteristic phases of the splitting process are depicted in Fig. 1. A fully developed finger is accompanied by convection rolls, two of which are centered at the reaction front [Fig. 1(a)]. A second pair of convection vortices lies outside the frame shown in Fig. 1(a), however, its existence is strongly supported by the flow lines at the bottom of Fig. 1. Inside the central part of the finger, close to the reaction front, the liquid moves upward and downward outside the finger. However, there is also a downward flow inside the finger and at its lower part, as seen at the very bottom of the image [Fig. 1(a)]. The upward and downward flows inside the finger are separated by a stagnation point which has saddle-node characteristics. The onset of finger splitting takes place at the flattest part of the front, i.e., at its top [at $t \sim 151$ s, Fig. 1(b)]. Interestingly, however, the macroscopic flow field is still very similar to that at $t=86$ s [Fig. 1(a)]. There are two convection rolls above the reaction front as well as a descending flow in the lower part of this image [Fig. 1(b)], which again indicates the existence of a second pair of convection rolls at a deeper position in the Hele-Shaw cell. Unfortunately, the second pair of convection rolls cannot be fully visualized due the limited observation area, which results from the requirement of a simultaneous detection of the tracer particle motion as well as of the dynamics of the reaction front. The flow fields at $t=236$ and 296 s [Figs. 1(c) and 1(d), respectively] show the behavior after finger splitting. In the reaction front a new valley between two new fingers is already formed at $t \sim 236$ s [Fig. 1(c)] and it is clearly developed at $t=296$ s [Fig. 1(d)]. A new set of macroscopic convection rolls is observed at $t \sim 236$ s and it becomes fully developed at $t \sim 296$ s.

To clarify how a finger splits and how the macroscopic flow fields at the reaction front rearrange, the section of the front where finger splitting occurs is presented in detail in Fig. 2. Before splitting, the reaction front possesses a homogeneous curvature, as seen from the good match between the reaction front and the radius of a circle drawn in Fig. 2(a). The flow-field vectors, and hence the magnitude of the flow inside the finger, are mostly smaller than those outside. The largest vectors point to the valleys between two neighboring fingers. Inside the finger, the flow vectors point upwards, mostly to the northeast. The fluid moves upward inside the finger, crosses the front, and turns down above the finger. This corresponds to the upper pair of convection rolls shown in Fig. 1.

The fingertip splitting occurs between $t=109$ s [Fig. 2(a)] and $t=151$ s [Fig. 2(b)]: at $x \sim 5$ mm, the front begins to lag behind the rest of the propagating front, leading to the formation of a "valley" or cusp, which separates the two newly formed fingers from each other. With time, this cusp evolves and so do the new fingers [Figs. 2(b)–2(d)]. Let us now focus on the array of flow vectors. Shortly after the onset of finger splitting [$t=151$ s, Fig. 2(b)], the overall flow picture is strongly reminiscent of the flow field observed before splitting [at $t=109$ s, Fig. 2(a)]. There is, though, a small but important difference: the flow vectors determined at the wake of the forming cusp (4 mm$\leqslant x \leqslant$6 mm) are shorter than those in the regions where the new fingers grow (at $x=3$ mm and 7 mm$\leqslant x \leqslant$10 mm).

The macroscopic changes in topology of the orientation of the flow vectors is evident at $t \sim 223$ s [Fig. 2(d)]. All of the vectors above the finger point downwards; to the southwest in the left part and to the southeast in the right part of the image. Most of the vectors inside the finger point to the east and only a few vectors point to the north or northeast. The

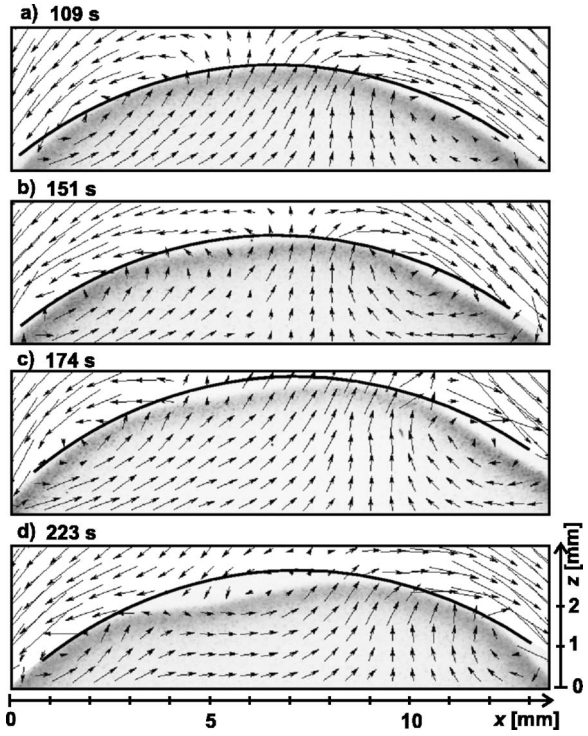

FIG. 2. Details of the finger splitting and adjacent flow-field development. (a) A fully developed finger is associated with two convection rolls located at the reaction front ($t=109$ s). (b) At $t\sim 151$ s the finger splits. (c) At $t\sim 174$ s the splitting becomes more pronounced. The macroscopic flow-field pattern is quite reminiscent to the situation prior to finger splitting. (d) At $t=223$ s, the macroscopic flow field is being rearranged, forming a new macroscopic convection roll. The black lines at the reaction front are segments of a circle and are intended as a guide for the eyes, to help to visualize the finger-splitting process. The arrows represent vectors of the hydrodynamic flow field; they show the direction and magnitude of the flow.

formation of a new convection roll can be seen in the second and third rows of the flow vectors at 5 mm$\leqslant x\leqslant$8 mm.

The general behavior observed in finger-splitting experiments can be summarized as follows: Fully developed fingers are accompanied by two pairs of convection rolls: while one pair is visible in Fig. 1 centered at the reaction front, the second pair of vortices is located well below the front, below a stagnation point (Fig. 1). When the finger becomes large enough, splitting starts at extended, almost horizontal segments of the fingertip. This is associated with small fluctuations of the flow fields in the immediate vicinity of that part of the front where the new cusp develops. Once a finger has split, the new fingers expand and become larger, while the cusp separating them also evolves. When the cusp is deep enough, the macroscopic hydrodynamic flow field is seen to rearrange and a new convection roll develops.

III. MODEL

To understand the experimental flow dynamics and, in particular, the existence of two pairs of convection rolls, we study numerically the problem focusing on a reaction-diffusion-convection model for an exothermic reaction, as it is the case for the IAA reaction. The dimensionless equations describing the system are [11]

$$\nabla p = -\mathbf{u} + [(1-C) + \gamma_T T]\mathbf{i}_x, \tag{4}$$

$$\rho = (1-C) + \gamma_T T, \tag{5}$$

$$\nabla \cdot \mathbf{u} = 0, \tag{6}$$

$$\frac{\partial C}{\partial t} + \mathbf{u}\cdot\nabla C = \nabla^2 C - \mathrm{Da}C(C-1)(C+d), \tag{7}$$

$$\frac{\partial T}{\partial t} + \mathbf{u}\cdot\nabla T = \mathrm{Le}\nabla^2 T - \mathrm{Da}C(C-1)(C+d) - \alpha T. \tag{8}$$

The geometry considered is a two-dimensional (2D) Hele-Shaw cell oriented vertically along the gravity field $\mathbf{g}$ directed along x (y being the transverse direction) and thin enough so that the velocity field $\mathbf{u}=(u_x,u_y)$ of the incompressible flow is described by 2D Darcy's law (4). C corresponds to the concentration of the autocatalytic species and its evolution is given by the solution of the reaction-diffusion-convection equation (7). The exothermic reaction triggers a temperature distribution governed by the energy balance in Eq. (8), which incorporates convective and diffusive transport terms, heat production by the reaction, and heat losses through the walls approximated by Newton's law of cooling. The Newton coefficient α is a composite coefficient that measures the rate of heat transfer from the liquid to the wall, through the wall, and from the wall to the surrounding air. The model depends on four dimensionless parameters: the first one Da, the Damköhler number, is defined as the ratio between the characteristic hydrodynamic time scale and the chemical time scale. The three other parameters related to heat are the overall heat-transfer coefficient α measuring the intensity of the heat losses, the Lewis number Le, which is defined as the ratio between the thermal diffusivity D_T and the molecular diffusivity D, and γ_T the thermal expansion coefficient quantifying the density change due to the temperature jump across the front. As density decreases with temperature, we have $\gamma_T<0$.

In the absence of flow, the base state of the system is a concentration RD front solution [15] of Eq. (7) corresponding to the products at $(C,T)=(1,1)$ invading the reactants at $(C,T)=(0,0)$. The dimensionless density $\rho=1-C+\gamma_T T$ therefore decreases when going from the density of the reactants $\rho_r=1$ to that of the products $\rho_p=\gamma_T<0$ such that ascending fronts are buoyantly unstable here.

In the case of insulating walls ($\alpha=0$) the heat profile follows the concentration profile but is spatially more spread out for values of the Lewis number Le>1 as the heat then diffuses faster than the chemical species. In the case of heat-conducting walls ($\alpha\neq 0$) the temperature profiles are pulses as the heat produced in the front is subsequently dissipated through the walls behind it. Equations (4)–(8) are integrated using the numerical technique [16], periodic boundary conditions, and initial conditions as detailed in Ref. [11]. A quantitative comparison with the experiments is difficult as un-

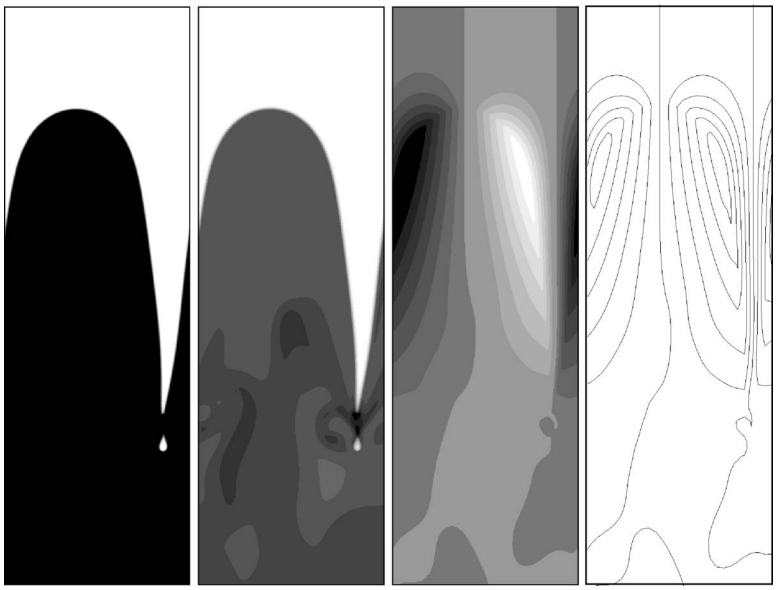

FIG. 3. Density plots of the single-finger asymptotic dynamics of the fingering of a chemical front in an insulated system for $\alpha=0$ showing from left to right at a time $t=1300$ the concentration C, the temperature T, the stream function ψ, and the isovelocity lines.

certainties remain regarding the exact experimental values of Da, γ_T, and α. We use, therefore, values of parameters in the range of possible experimental values [3,10,11]. The parameters used here are Da=0.5, $d=0.0021$, Le=3, $\gamma_t=-3$ in a system of dimensionless width 768 with $\alpha=0$ for insulating walls and $\alpha=0.01$ for conducting walls. It has been shown previously [11] that heat losses through the walls change the nonlinear dynamics compared to the case of insulating walls not leading to one single finger as in the isothermal case [3] but to increased tip splitting. Integrating Eqs. (4)–(8) first in the absence of thermal leaks, i.e., setting the coefficient α to zero, the nonlinear dynamics leads indeed for periodic boundary conditions to a single finger as shown in Fig. 3(a). This figure displays the concentration field C on a gray scale ranging from the product concentration $C=1$ in black to the fresh reactants $C=0$ in white. Figure 3(b) shows the corresponding temperature profile, with the temperature of the product solution in black while the room temperature $T=0$ of the reactants is displayed in white. The corresponding stream function ψ (such that $u_x=\psi_y$ and $u_y=-\psi_x$) and convection rolls are plotted in Figs. 3(c) and 3(d), respectively. We see that, for insulating walls, the flow field around the finger has the form of two convection rolls, a situation similar to that obtained in the isothermal case. The light and hot product solution behind the front rises in the middle of the finger and the two corresponding counter-rotating convection rolls close in dragging down on the side of the fingers the heavier and cooler fresh reactant solution.

The situation is quite different in the case of conductive walls as can be seen in Fig. 4. Here, all parameters are the same as in Fig. 3 except that now $\alpha=0.01$. We observe that fingering in the presence of heat losses is quite different not leading to one single smooth finger but to a finger featuring tip splitting. Focusing on Fig. 4(b), it is seen that the temperature profile is not a front anymore as in the insulating case but is now a pulse surrounding the concentration front. The fresh reactants are at room temperature ($T=0$), then heat is produced by the reaction occurring at the front (black zone) but is lost at the wake of the front because of heat dissipation through the walls. Products far behind the wake of the front have thus cooled down to $T=0$. Analysis of the stream function and flow field in Figs. 4(c) and 4(d) reveals that in addition to convection rolls around the fingers, two counter-rotating vortices also exist behind the front in the bulk. As a consequence, in the upper part of the finger, fluid is rising in the middle of the finger and flows down in the valley between the fingers, while in the lower part of the finger, the middle of the fingers is characterized by a downflow. This four-vortices situation, which remains in the course of the dynamics (see Fig. 5), induces a saddle-node

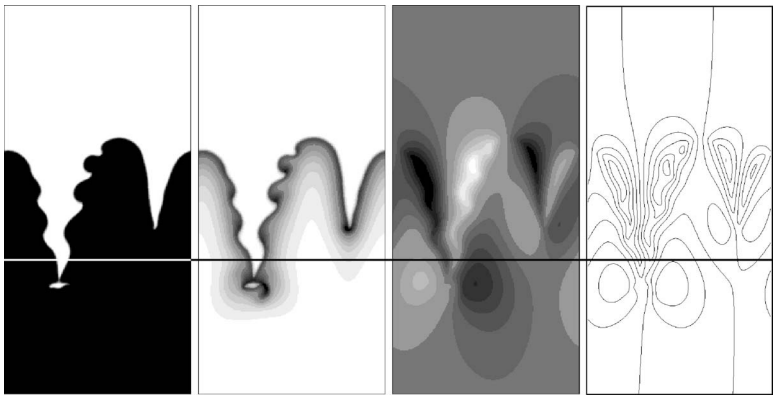

FIG. 4. Density plots of the tip-splitting dynamics of the fingering of a chemical front in a system with conductive walls for $\alpha=0.01$ showing from left to right the concentration C, the temperature T, the stream function ψ, and the isovelocity lines at time $t=1700$.

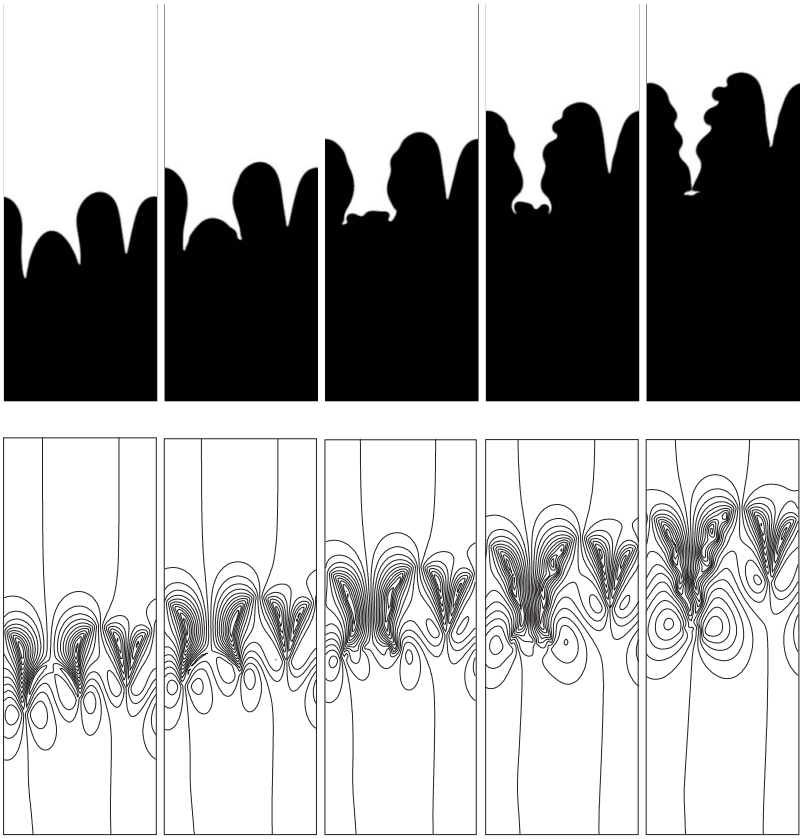

FIG. 5. Evolution of the concentration (upper line) and of the velocity field (lower line) showing the onset of tip splittings for $\alpha=0.01$ from $t=1300$ to $t=1700$.

configuration of the velocity vectors as can clearly be seen in Fig. 6. The similarity between the saddle-node configuration of the flow field observed in the experiment (Figs. 1 and 2) and in the numerical simulation in the case of conducting walls suggests that heat losses are important in understanding the details of the experimental flow field.

To clarify the influence of heat effects in the generation of tip splitting, it is useful to recall that in this system the vorticity of the flow is generated by gradients of concentration and temperature transverse to the direction of propagation of the front. Indeed, taking the curl of equation Eq. (4) to eliminate the pressure [17], we find that the vorticity ω is equal to

$$\omega = \nabla^2 \psi = -C_y - |\gamma_T| T_y, \tag{9}$$

where the subscript y indicates a derivative with regard to the y direction. A close inspection of Fig. 3 shows that, in the case of insulating walls, the gradients of concentration C_y and of temperature T_y along a horizontal line crossing the finger both have the same positive sign in the left-half part of the finger. This generates a negative vorticity responsible for the large counterclockwise rotating vortex bringing fluid upwards in the middle of the finger and turning then to the left [see the black vortex in the stream function in Fig. 3(c)]. By symmetry, the negative gradients of C and T in the right half of the finger generate a positive vorticity [see the white vortex in the stream function in Fig. 3(c)] at the origin of the large vortex turning clockwise in the right part of the finger. We can also easily understand the fact that there are two vortices inside one finger as, when going from one valley where $(C,T)=(0,0)$ to the next one by crossing horizontally the product zone where $(C,T)=(1,1)$, the gradient of C_y and T_y both change sign twice. This fact, along with the incompressibility of the fluid, induces the existence of two counter-rotating vortices.

The situation is quite different in the presence of heat losses because now the temperature profile is not a front anymore but a pulse of heat localized around the front. While the source of vorticity related to the gradient of concentration C_y is the same as before, the gradient of temperature is now stronger because the localized zone of heat around the front implies the same change of T from 0 to 1 but on a smaller distance. In addition, the pulse of heat localizes the vorticity around the reaction zone. As the strength of the flow circulation is related to the magnitude of the T gradient, the temperature pulse (a source of enhanced localized vorticity) favors tip splitting [17,18]. In addition to those small localized sources of vorticity at the front, the general structure of the temperature profile now also induces the presence of a quadrupole structure in the flow field. Along the horizontal line drawn in Fig. 4, the temperature gradient changes sign four times across one finger when going, in the left part, from the reactant in the valley at $T=0$ to the reaction front at $T=1$ then back to cooled products at T close to zero in the middle of the finger. The same changes then occur again in the right part of the finger. This explains the existence of four successive counter-rotating vortices when crossing one finger horizontally. Going down a vertical line in the middle of one finger, the temperature field goes from $T=0$ in the fresh reactants at room temperature to the cooled products also at $T=0$ by passing through a localized hot zone at $T=1$. As the

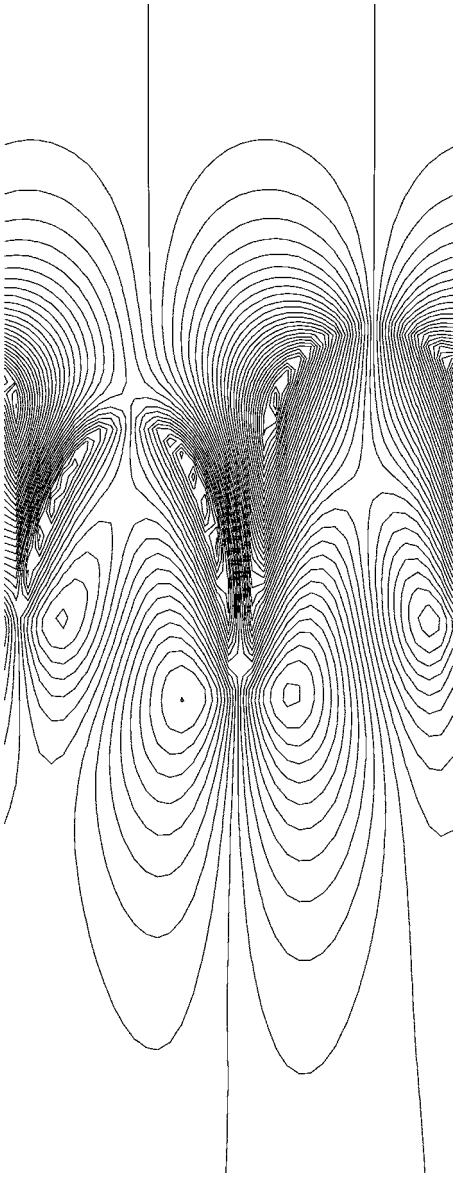

FIG. 6. Reconstructed numerical velocity field in the case of conducting walls ($\alpha=0.005$) at time $t=1800$. The general quadrupole structure as well as the saddle-node point are clearly visible in the center of each finger. Little vortices favoring tip splittings can be seen inside the reaction zone.

fluid is incompressible, such a change leads to two zones of counter-rotating vortices.

As a summary, at isothermal conditions or in exothermic systems with insulating walls, the nonlinear evolution of fingers is towards general coarsening. Tip splittings can occur for large values of the Damköhler or Rayleigh numbers [3]. We have shown here that the change of the temperature profile from a front to a pulse when heat losses are present implies increased vorticity close to the interface, which favors tip splitting. Tip splittings will thus be more often observed in systems with conducting walls with regard to insulating ones, all other parameters being the same. Moreover, the general structure of the flow field inside one finger changes from a two-vortices structure to a quadrupole one.

IV. DISCUSSION

The experimental and numerical studies presented here focus on the phenomenon of finger splitting occurring in slightly exothermic ascending fronts of the IAA reaction, when the Rayleigh-Taylor hydrodynamic instability is well developed, i.e., in the so-called nonlinear regime.

In experiments, the dynamics of the reaction front and the displacement of buoyant tracer particles were monitored simultaneously. PIV analysis of the motion of the tracer particles allows for the reconstruction of the hydrodynamic flow fields associated to the front dynamics. This now makes accessible the visualization of the flow fields in an experimental reaction-diffusion system subject to Rayleigh-Taylor instabilities in a Hele-Shaw cell arrangement.

A fully developed reaction front finger is associated to a flow field organized around a saddle node that is positioned in the interior of the finger at a certain distance from the front. This saddle node separates the domains of two pairs of convection rolls, which in turn embed the finger. The first pair of convective vortices is centered at the reaction front (fingertips, Fig. 1), while the second pair is inferred to be located below the domain of the saddle node. Unfortunately, the desirable increase in the area of experimental observation to capture this pair of convective vortices is hampered by the resolution required to follow the motion of the tracer particles.

Numerical simulations have been performed using a minimal model for the dynamics of the IAA system in a Hele-Shaw configuration, which takes into account effects of heat production at the reaction front and that of heat dissipation through the reactor walls. Flow fields consisting of four convective vortices organized around a saddle node located inside the reaction front finger could be obtained only if the heat production at the exothermic reaction front and the heat dissipation through the reactor walls were explicitly considered. The calculated flow fields are in good qualitative agreement with those observed experimentally.

The importance of considering both the solutal and thermal effects in modeling the finger development can be assessed by comparing the present numerical results with those published earlier in literature. Calculations that assume that the density difference along the reaction front is solely due to changes in the chemical composition, or that neglect the tiny thermal effects [3,19–23] as well as studies considering only thermal effects [24,25], predict a flow field consisting of a single pair of convection rolls. Interestingly, a study attributing the density differences exclusively to thermal effects, thereby omitting any solutal contributions to the changes in density [25], shows that flow fields involving one, two, or even three pairs of convection rolls may be obtained, depending on the selected eigenmode of finger growth. However, the most unstable mode is always the one featuring two convection rolls. Moreover, the flow fields with more convection rolls neither really correspond to the situation seen in the experiment, nor to those obtained in our numerical simulations. In addition, this model does not reflect the effective physical mechanism, where both solutal and thermal effects contribute to the density changes at the reaction front.

The numerical calculations presented in Sec. III indicate that the resulting hydrodynamic flow fields are highly sensi-

tive to small changes in the heat-related parameters. Thus, moderate changes in the Newton heat-transfer coefficient α already drastically modify the structure of the flow field: While for $\alpha=0$ only a single pair of convection rolls is obtained, the slight increase to $\alpha=0.005$ or 0.01 already leads to a very different hydrodynamic situation, namely, the existence of two pairs of vortices surrounding a finger (Figs. 3–6). Thus, even the very weak exothermicity of the IAA recipes used, which may lead to tiny temperature jumps at the reaction front of as much as $\Delta T \leqslant 0.1$ K may be sufficient to induce the more complex hydrodynamic quadrupole vortex-patterned flow field. This suggests that even though heat production and dissipation appear to be negligibly small, they cannot be omitted even for a reaction with such a small exothermicity as the IAA system.

Even though there is very good agreement between our heat-loss-containing model and the experimental observation in the finger-splitting phenomena, small differences may persist between the experimental and numerical results. For instance, in the model calculations, the loci of finger splitting are slightly shifted towards the sides of a finger, as compared to the experiments where this happens on the flattest part of the fingertip. However, these differences are most probably connected to the complexity of the observed phenomena that we wish to describe by a minimal model, and to the choice of the values of model parameters, which very often need to be estimated.

V. CONCLUSIONS

The dynamics of splitting of the slightly exothermic reaction front fingers was studied in a vertically oriented Hele-Shaw cell. By the simultaneous observation of the wave front and a particle-imaging velocimetry analysis (PIV) of tracer particles, we have obtained the details of the experimental flow field inside one finger of an autocatalytic ascending IAA front undergoing a Rayleigh-Taylor instability. This flow field is characterized by a saddle-node structure separating the upper part of the finger where the flow goes up in the middle of the finger to turn sideways close to the tip. In the lower regions of the finger, the flow moves down in the opposite direction. This leads to a flow field where every well-developed finger is embedded between four vortices of the hydrodynamic flow. The numerical integration of a simple reaction-diffusion-convection model that takes into account the temperature field due to the exothermicity of the reaction shows that the quadrupole structure of the experimental flow field requires the presence of heat losses through the reactor walls. Indeed, in insulated systems, the temperature profile is a front that combines with the concentration front to yield only two counter-rotating vortices in one finger. By contrast, in the presence of heat losses through the walls, the temperature profile becomes a pulse centered around the reaction zone. This localized heating pulse provides an increased source of vorticity favoring tip splitting in the reaction zone and a quadrupole structure of the general flow field.

ACKNOWLEDGMENTS

We would like to thank A. Zebib and E. Meiburg for fruitful discussions. J.D. was supported by FRIA (Belgium), and L.S. was supported by the Deutsches Zentrum für Luft- und Raumfahrttechnik (DLR). This work was sponsored by ESA, Prodex (Belgium), DLR (Germany), the Communauté française de Belgique under the "Actions de Recherches Concertées" Programme, as well as the Bundesministerium für Wirtschaft und Technologie (Germany).

[1] I. R. Epstein and J. A. Pojman, *An Introduction to Nonlinear Dynamics: Oscillations, Waves, Patterns and Chaos* (Oxford University Press, New York, 1998).
[2] J. A. Pojman and I. R. Epstein, J. Phys. Chem. **94**, 4966 (1990).
[3] A. De Wit, Phys. Fluids **16**, 163 (2004).
[4] J. A. Pojman, I. R. Epstein, T. J. McManus, and K. Showalter, J. Phys. Chem. **95**, 1299 (1991).
[5] J. Masere, D. A. Vasquez, B. F. Edwards, J. W. Wilder, and K. Showalter, J. Phys. Chem. **98**, 6505 (1994).
[6] M. R. Carey, S. W. Morris, and P. Kolodner, Phys. Rev. E **53**, 6012 (1996).
[7] M. Böckmann and S. C. Müller, Phys. Rev. Lett. **85**, 2506 (2000).
[8] M. Böckmann and S. C. Müller, Phys. Rev. E **70**, 046302 (2004).
[9] J. Martin, N. Rakotomalala, D. Salin, and M. Böckmann, Phys. Rev. E **65**, 051605 (2002).
[10] A. De Wit, Phys. Rev. Lett. **87**, 054502 (2001).
[11] J. D'Hernoncourt, S. Kalliadasis, and A. De Wit, J. Chem. Phys. **123**, 234503 (2005).
[12] A. Hanna, A. Saul, and K. Showalter, J. Am. Chem. Soc. **104**, 3838 (1982).
[13] J. H. Merkin and H. Ševčíková, Phys. Chem. Chem. Phys. **1**, 91 (1999).
[14] L. Forštová, H. Ševčíková, M. Marek, and J. H. Merkin, Chem. Eng. Sci. **55**, 233 (2000).
[15] A. Saul and K. Showalter, in *Oscillations and Traveling Waves in Chemical Systems*, edited by R. J. Field and M. Burger (Wiley, New York, 1985).
[16] C. T. Tan and G. M. Homsy, Phys. Fluids **31**, 1330 (1988).
[17] G. M. Homsy, Annu. Rev. Fluid Mech. **19**, 271 (1987).
[18] R. Demuth and E. Meiburg, Phys. Fluids **15**, 597 (2003).
[19] J. Huang, D. A. Vasquez, B. F. Edwards, and P. Kolodner, Phys. Rev. E **48**, 4378 (1993).
[20] D. A. Vasquez, J. M. Littley, J. W. Wilder, and B. F. Edwards, Phys. Rev. E **50**, 280 (1994).
[21] Y. Wu, D. A. Vasquez, B. F. Edwards, and J. W. Wilder, Phys. Rev. E **52**, 6175 (1995).
[22] D. A. Vasquez, J. W. Wilder, and B. F. Edwards, J. Chem. Phys. **104**, 9926 (1996).
[23] J. Huang and B. F. Edwards, Phys. Rev. E **54**, 2620 (1996).
[24] B. F. Edwards, J. W. Wilder, and K. Showalter, Phys. Rev. A **43**, 749 (1991).
[25] J. W. Wilder, B. F. Edwards, and D. A. Vasquez, Phys. Rev. A **45**, 2320 (1992).